



## Article

# Study on the Response of the Summer Land Surface Temperature to Urban Morphology in Urumqi, China

Jiayu Fan <sup>1,2</sup> , Xuegang Chen <sup>1,2,\*</sup> , Siqi Xie <sup>1,2</sup> and Yuhu Zhang <sup>3</sup>

<sup>1</sup> School of Geographical Science and Tourism, Xinjiang Normal University, Urumqi 830054, China; fanjiayu@stu.xjnu.edu.cn (J.F.); xsqaiqi@126.com (S.X.)

<sup>2</sup> Xinjiang Key Laboratory of Lake Environment and Resources in Arid Zone, Urumqi 830054, China

<sup>3</sup> College of Resource Environment and Tourism, Capital Normal University, Beijing 100048, China; yuhu.zhang@cnu.edu.cn

\* Correspondence: caschxg@126.com; Tel.: +86-138-9991-0696

**Abstract:** Increases in urban temperature affect the urban ecological environment and human health and well-being. In urban morphology, building characteristics are important factors affecting the land surface temperature (LST). Contemporary research focuses mainly on the effects of land use, urban tissue configuration, and street networks on the LST, and the effects of building characteristics on the LST need to be further understood. The mean LST and the urban morphology indicators of a single grid were calculated via a remote sensing inversion and a spatial analysis, and a geographically weighted regression (GWR) model was established to explore the influence of the building coverage ratio (BCR), mean building height (BH\_mean), floor area ratio (FAR), and mean sky view factor (SVF\_mean) on the LST. The results show that the correlations between the urban morphology indicators and the LST at a scale of 100–500 m are of different degrees, and the correlations are more significant at a scale of 200 m. Therefore, the optimal spatial scale for studying the influence of urban morphology indicators on the LST is 200 m. The fitting effect of the GWR model is significantly better than that of the ordinary least squares (OLS) method, and the effects of each indicator on the thermal environment have spatial non-stationarity. The BCR, BH\_mean, FAR, and SVF\_mean differ in their ability to raise and lower the temperature in different spatial zones, and the order of influence is as follows: BCR > SVF\_mean > FAR > BH\_mean. This study will provide a reference for the urban planning of Urumqi.

**Keywords:** urban morphology; land surface temperature; mono-window algorithm; GWR; Urumqi



**Citation:** Fan, J.; Chen, X.; Xie, S.; Zhang, Y. Study on the Response of the Summer Land Surface Temperature to Urban Morphology in Urumqi, China. *Sustainability* **2023**, *15*, 15255. <https://doi.org/10.3390/su152115255>

Academic Editors: Alimujiang Kasimu and Liwei Zhang

Received: 6 August 2023

Revised: 2 October 2023

Accepted: 11 October 2023

Published: 25 October 2023



**Copyright:** © 2023 by the authors. Licensee MDPI, Basel, Switzerland. This article is an open access article distributed under the terms and conditions of the Creative Commons Attribution (CC BY) license (<https://creativecommons.org/licenses/by/4.0/>).

## 1. Introduction

The United Nations Human Settlements Programme (UN-Habitat), in the context of the topic of climate change, states that the effects of urbanization and climate change are converging in dangerous ways. Global warming is likely to reach 1.5 °C between 2030 and 2052 and will reach approximately 3 °C in 2100 based on current national government commitments [1]. Changes in land use due to urbanization represent one of the main causes of global warming [2]. In the process of urbanization, natural surfaces are replaced by impervious surfaces, which reduce latent heat flux and increase heat absorption in urban areas. The morphology of the urban surface leads to an increase in roughness, which reduces the urban ventilation performance of the city. In addition, the release of heat from human activities increases the accumulation of heat. The combined effect of these factors results in the urban heat island (UHI) effect [3,4]. Serious UHIs will threaten the sustainable development of cities, reduce thermal comfort, affect the health of urban residents, reduce urban air quality, and exacerbate urban ecological problems [5–7]. As the largest developing country in the world, China's urbanization rate is significantly higher than that of other developing countries [8], increasing from 17.92% in 1978 to 65.22% in 2022, and is expected to reach 80% by 2050 [9]. The UHI effect, triggered by the explosion in growth of the

urban population and massive development and construction, has become a major problem affecting the ecological environment and sustainable development in China [10]. Therefore, exploring influencing factors and strategies for mitigating UHI is crucial for improving residents' outdoor comfort, reducing energy consumption, minimizing air pollution and promoting healthy and low-carbon urban development.

Urban morphology refers to the physical characteristics of urban forms, such as the spatial layout of buildings and the urban landscape and its transformations [11]. Zhang et al. [12] classified urban morphology indicators into six categories: urban tissue configuration, street networks, building plot characteristics, land use, natural features, and urban growth. The current research focuses more on urban tissue configuration, street networks, and land use; research on land use with respect to these three aspects began earlier, and the results are more abundant. Some examples include the variability in LSTs of different land-cover-types [13–15] or the effects of landscape patterns on LSTs, referring to quantitative land-cover-type proportions and structures [16,17]. These previous studies have neglected the importance of building plot characteristics. Building plot characteristics are important physical characteristics of urban morphology, and factors such as building density, orientation, and height affect local and city-scale surface energy balance processes and air flow, change the thermal environment within the city, and may exacerbate the UHI effect [18]. Chen et al. [19] assessed the influence of urban spatial pattern indicators on the LST from three dimensions and found that mean building height (MAH) has a cooling effect on the LST, and the relationship between patch density (PD), the landscape shape index (LSI), Shannon's diversity index (SHDI), the contagion index (CONTAG), people density (POD), FAR, and the LST varies with the seasons. The degree of influence on the LST can be ranked as follows: building morphology > landscape pattern > social development. Liu et al. [20] explored the effects of the BCR, building volume density (BVD), and frontal area index (FAI) on the LST and found that the BCR is an important urban morphology indicator affecting the LST, followed by BVD and FAI. Zhang et al. [21] showed that three-dimensional (3D) building forms had a significant effect on the LST, with BD being the most important factor influencing the LST, and the hierarchy of effects on the LST was as follows: building form > landscape type > land cover type > social development. Qiao et al. [22] established an urban ventilation network model (UVNM) to explore the effects of urban morphology and building height on urban ventilation. The results showed that considering the direction and frequency of wind in urban design based on urban morphology and building height can effectively optimize ventilation and adjust urban environmental problems. He et al. [23] verified that the morphological characteristics of a compact, high-rise gridiron precinct had strong modification effects on the precinct's ventilation. The precinct's ventilation performance under the influence of a sea breeze could significantly mitigate the UHI and improve the relative humidity and then significantly improve outdoor thermal comfort. It has been shown that 3D building plot characteristics are important factors affecting the LST, but the current research on 3D building plot characteristics is still relatively limited, and the existing studies mainly focus on subtropical monsoon climate zones and temperate monsoon climate zones, e.g., Shanghai, Beijing, Guangzhou, etc., while less attention has been paid to cities in temperate continental arid climate zones.

The Landsat series of satellites has become one of the most effective sources of remote sensing data in the study of monitoring the state of the land's surface and changes in the surface over a long period of time due to the high spatial resolution and spectral information of the data, as well as its many advantages, such as the continuous observation of the Earth. The thermal infrared band is also widely used in the monitoring of changes in the LST because it is sensitive to the thermal radiation information of ground objects [24]. Scholars have proposed different algorithms for LST inversion, which mainly include the single-channel method [25], the mono-window algorithm [26], the split-window algorithm [27], and the atmospheric correction method based on the radiative transfer equation [28]. Some scholars have proven that the accuracy and inversion precision of the mono-window algorithm is higher compared to other algorithms [29,30]. Therefore, in this paper, we

refer to the study by Hu et al. [31] for the LST inversion of the 10th band of the Landsat OLI/TIRS instruments using the mono-window algorithm.

The research methods for the association between urban morphology and LST include global linear regression analysis as well as spatial regression analysis. The most commonly used global linear model is OLS, e.g., Su et al. [32] used a linear regression model to explore the effects of urban morphology on LST in 266 cities, and the results showed that, nationwide, LST (in summer) was negatively correlated with urban compactness, boundary complexity and urban shape, but positively correlated with proximity correlation, and these effects are different between cities. In recent years, some studies have shown that there is spatial autocorrelation in LST, the effects of urban morphology indicators on LST vary spatially, and global linear regression analysis is invalid. Many scholars now use spatial regression analysis models for research, such as Yin et al. [33], who compared a spatial error model (SEM) and a spatial lag model (SLM) and found that the parameters of the SEM model were better than the SLM model. Zhang et al. [34] used least squares with GWR to assess the relationship between LST and 3D urban morphology at the community level in Phoenix, Arizona, USA, and demonstrated that GWR further improves compared to OLS regression model fitting. Spatial regression modeling can reveal the spatial heterogeneity of urban morphology elements on LST, and therefore, spatial analysis is a more mainstream approach for such studies.

Based on this, this paper uses remote sensing inversion to decipher the LST in the central urban area of Urumqi, quantifies the characteristics of urban morphology using GIS and establishes a GWR model to explore the influence of urban morphology on LST, with the following research objectives: (1) To use Urumqi, an oasis city in the arid zone of temperate continental climate, as an example for the inversion of the LST of the central urban area and the analysis of the characteristics of the spatial distribution of LST in Urumqi by combining the elements of urban morphology. (2) To find the optimal spatial scale for the study of the correlation between urban morphology and LST in Urumqi by comparing the different spatial scales and exploring the spatial distribution of the urban morphology based on the optimal study scale. (3) To use the GWR model to analyze how the impact of urban morphology indicators on LST varies spatially. Understanding the influence of urban morphology on LST at the urban scale will help city managers and planners optimize the urban thermal environment and promote sustainable urban development.

## 2. Methods

### 2.1. Study Area

The city Urumqi ( $86^{\circ}37'33''$ ~ $88^{\circ}58'24''$  E,  $42^{\circ}45'32''$ ~ $44^{\circ}08'00''$  N) is located in the northern foothills of the middle section of the Tianshan Mountains and the southern edge of the Junggar Basin and is the capital of the Xinjiang Uygur Autonomous Region, China, as well as one of the largest arid-zone oasis cities of Central Asia. In terms of climatic conditions, the city has a mid-temperate continental arid climate with scarce rainfall, average annual precipitation of 236 mm, short spring and fall seasons, long summer and winter seasons, and average temperatures of  $-15.2$  °C (January) and  $25.7$  °C (July). June, July, and August are summer months, and the north and northwest winds prevail in the built-up areas in summer. The Urumqi area is surrounded by mountains on three sides, with an average elevation of 800 m above sea level, and is now under the jurisdiction of seven districts and one county: Toutunhe district, Xinshi district, Midong district, Shayibake district, Shuimogou district, Tianshan district, Dabancheng district, and Urumqi County, with a total area of  $13,800$  km<sup>2</sup>, of which the built-up area is  $522$  km<sup>2</sup>. Over the past 20 years, Urumqi has experienced a rapid urbanization process, with GDP increasing from  $\text{CNY } 315 \times 10^8$  in 2001 to  $\text{CNY } 3691.57 \times 10^8$  in 2021, and the number of residents in the populations increasing rapidly from  $169.03 \times 10^4$  to  $407 \times 10^4$  during the same period. The substantial increase in population size, the replacement of natural surfaces with a large number of impervious surfaces, and the anthropogenic heat generated by human activities have led to an increase in the overall level of thermal emissions in the city, resulting in

a series of derivative problems in the thermal environment. The study selected a more densely built-up area in the center of Urumqi, covering an area of approximately 111.3 km<sup>2</sup> (Figure 1), including parts of the Xinshi district, the Midong district, the Shuimogou district, the Shayibake district, and the Tianshan district.

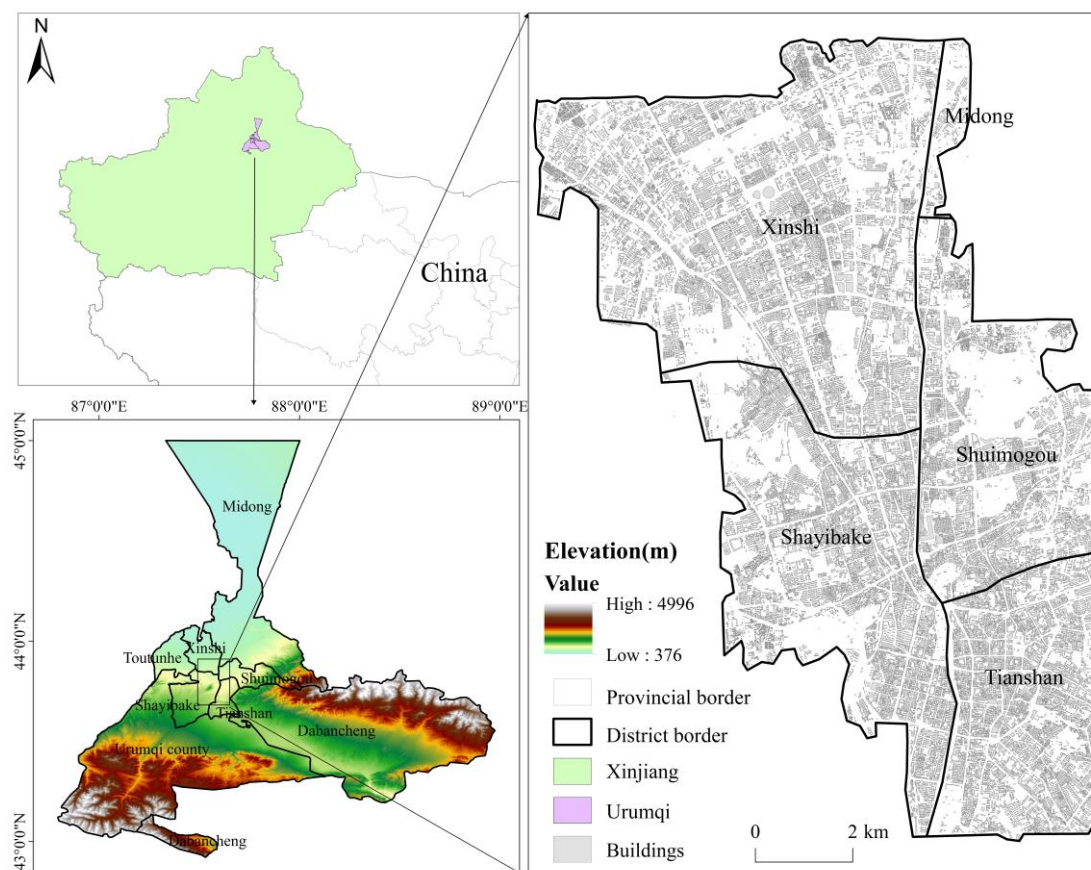


**Figure 1.** Study area.

## 2.2. Data Sources and Pre-Processing

The administrative boundary and road network data used in this paper are from the National Catalogue Service for Geographic Information and Digital Elevation Model (DEM) data from the Geospatial Data Cloud website. This paper uses Landsat 8 OLI/TIRS image data sets from the official website of USGS. We selected three images covering the central urban area of Urumqi on 15 July 2020, 1 July 2021, and 4 July 2022, with transit times of 04:55:47, 04:55:49, and 04:56:10, and Beijing times of 12:55:47, 12:55:49, and 12:56:10, path: 143, row: 29, and the spatial resolution is 30 m. All Landsat images were radiometrically calibrated and cropped by ENVI 5.3 for predominantly LST inversion. The building vector data in the center of Urumqi city were obtained from Tianditu (including building height attributes). ArcGIS 10.2.0.3348 was used to add fields in the data attribute table, and the footprint area of each building was calculated using the computational geometry tool. Assuming that the floor height of each building is 3 m, the field calculator is used to calculate the number of floors of each building and is mainly used to calculate the urban morphology indicators (Table 1).

**Table 1.** List of databases and sources used for this study.

Data Sets	Data Resources	Spatial Resolution
Administrative boundaries	<a href="https://www.webmap.cn/">https://www.webmap.cn/</a> (accessed on 20 January 2023)	-
DEM	<a href="https://www.gscloud.cn/">https://www.gscloud.cn/</a> (accessed on 20 January 2023)	30 m
Road data sets	<a href="https://www.webmap.cn/">https://www.webmap.cn/</a> (accessed on 20 January 2023)	-
Landsat 8 OLI/TIRS data sets	<a href="https://earthexplorer.usgs.gov/">https://earthexplorer.usgs.gov/</a> (accessed on 15 March 2023)	30 m
Building data sets	<a href="https://www.tianditu.gov.cn/">https://www.tianditu.gov.cn/</a> (accessed on 27 August 2022)	-

### 2.3. LST Inversion and Grading

#### 2.3.1. Top of Atmosphere (TOA) Spectral Radiance

Radiometric calibration of the thermal infrared band using radiance correction factors was used to convert DN values to TOA spectral radiances, i.e.,:

$$L_{\lambda} = M_L \times Q_{cal} + A_L, \quad (1)$$

where  $L_{\lambda}$  is the top of atmosphere spectral radiance ( $\text{W} \cdot \text{m}^{-2} \cdot \text{sr}^{-1} \cdot \mu\text{m}^{-1}$ ) in band  $\lambda$ ;  $M_L$  is the gain parameter;  $Q_{cal}$  is the image DN value (i.e., the gray value); and  $A_L$  is the offset parameter, where the  $M_L$  and  $A_L$  parameters can be obtained directly from the image metadata file.

#### 2.3.2. TOA Brightness Temperature

Using the value of the thermal constant in the metadata file, the radiant luminance was converted to luminance temperature according to Planck's law, i.e.,:

$$T_b = \frac{K_2}{\ln\left(\frac{K_1}{L_{\lambda}} + 1\right)}, \quad (2)$$

where  $T_b$  is the TOA brightness temperature (K); and  $K_1$  and  $K_2$  are constants. For TIRS sensor Band 10,  $K_1 = 774.89$  ( $\text{W} \cdot \text{m}^{-2} \cdot \text{sr}^{-1} \cdot \mu\text{m}^{-1}$ ) and  $K_2 = 1321.08$  K.

#### 2.3.3. Calculation of Surface-Specific Emissivity

A simpler method of estimating the composition ratio of mixed image elements was used to determine the surface composition ratio using empirical formulas for the calculation of surface ratio [35]. For urban areas, we simply categorized them into three types, water bodies, natural surfaces, and built-up surfaces, so the surface ratio radiance was estimated for the mixed image scale by the following equation:

$$\varepsilon = P_v R_v \varepsilon_v + (1 - P_v) R_m \varepsilon_m + d_{\varepsilon}, \quad (3)$$

where  $\varepsilon$  is the surface-specific emissivity of the hybrid image element;  $P_v$  is the vegetation cover;  $R_v$  is the temperature ratio of the vegetation;  $R_m$  is the temperature ratio of the building surface;  $\varepsilon_v$  is the surface-specific emissivity of the vegetation, for the OLI/TIRS 10th band data,  $\varepsilon_v = 0.98672$  and  $\varepsilon_m = 0.96767$ ; and  $d_{\varepsilon}$  is the radiative correction term, obtained from the empirical equation:

$$d_{\varepsilon} = 0.0038 P_v. \quad (4)$$

Using the results of Qin et al. [36], the temperature-specific emissivity of vegetation and building surfaces is:

$$R_v = 0.09332 + 0.585 P_v, \quad (5)$$

$$R_m = 0.9886 + 0.1287 P_v, \quad (6)$$

where the vegetation cover,  $P_v$ , can be calculated from the normalized vegetation index  $NDVI$ :

$$P_v = (NDVI - NDVI_S) / (NDVI_V - NDVI_S). \quad (7)$$

In the formula, the empirical values of  $NDVI_V = 0.70$  and  $NDVI_S = 0.05$  from Qin et al. [33] were used for estimation.

#### 2.3.4. Determination of Atmospheric Transmittance

The atmospheric transmittance was calculated with the website (<https://atmcorr.gsfc.nasa.gov/> accessed on 15 July 2023), using the following procedure: the upper atmospheric contours utilize the mid-latitude summer standard atmosphere; enter the time of Landsat 8 transit (to the minute), latitude and longitude, temperature ( $^{\circ}\text{C}$ ), relative humidity (%), altitude (km), and barometric pressure (mb) into the website; click on "Calculate" to obtain the atmospheric transmittance,  $\tau = 0.84$  for this study area.

#### 2.3.5. Calculation of the Mean Atmospheric Temperature

Under conditions where the weather is clear and there is no obvious atmospheric vertical vortex, the mean atmospheric temperature can be approximately calculated from the surface air temperature. The study area is located in the mid-latitude region, and the image acquisition time is summer, so we chose:

$$T_a = 16.0110 + 0.92621T_0, \quad (8)$$

where  $T_a$  is the mean atmospheric temperature (K) and  $T_0$  is the surface air temperature (K).

#### 2.3.6. LST Calculations

According to Qin et al. [26], the LST in degrees Celsius can be extracted from Landsat 8 OLI/TIRS data as follows:

$$LST = \left\{ \frac{a \times (1 - C - D) + [b \times (1 - C - D) + C + D] \times T_b - D \times T_a}{C} \right\} - 273.15, \quad (9)$$

$$C = \tau \times \varepsilon, \quad (10)$$

$$D = (1 - \tau)[1 + \tau(1 - \varepsilon)], \quad (11)$$

where  $a$  and  $b$  are constants,  $a = -67.355351$  and  $b = 0.458606$ ;  $T_b$  is the brightness temperature (K);  $T_a$  is the mean atmospheric temperature (K);  $\tau$  is the atmospheric transmittance;  $\varepsilon$  is the surface specific emissivity; and  $C$  and  $D$  are calculated for atmospheric transmittance,  $\tau$ , and surface specific emissivity,  $\varepsilon$ .

#### 2.3.7. LST Classification

In order to express the temporal and spatial distribution patterns of the surface heat field in the study area more intuitively, this paper adopts the standard deviation classification method [37] to classify the LST into six levels: low LST zone (LLZ), relatively low LST zone (RLLZ), medium LST zone (MLZ), relatively high LST zone (RHLZ), high LST zone (HLZ), and extremely high LST zone (EHLZ). The three-year summer mean LST value is  $39.89^{\circ}\text{C}$ , with a standard deviation of  $4.12^{\circ}\text{C}$ . The specific classification and calculations are shown in Table 2.

**Table 2.** Classification of LST based on standard deviation classification.

Grade	Grading Standard	Calculation Result
Low LST zone	$T_s \leq T_m - 2.5T_{std}$	$6.95 < T_s \leq 28.82$
Relatively low LST zone	$T_m - 2.5T_{std} < T_s \leq T_m - 1.5T_{std}$	$28.82 < T_s \leq 32.94$
Medium LST zone	$T_m - 1.5T_{std} < T_s \leq T_m - 0.5T_{std}$	$32.94 < T_s \leq 37.06$
Relatively high LST zone	$T_m - 0.5T_{std} < T_s \leq T_m + 0.5T_{std}$	$37.06 < T_s \leq 41.18$
High LST zone	$T_m + 0.5T_{std} < T_s \leq T_m + 1.5T_{std}$	$41.18 < T_s \leq 45.30$
Extremely high LST zone	$T_m + 1.5T_{std} < T_s \leq T_m + 2.5T_{std}$	$45.30 < T_s \leq 48.85$

$T_s$  represents LST,  $T_m$  represents mean LST,  $T_{std}$  represents standard deviation of LST.

#### 2.4. Selection and Calculation of Indicators

In this study, four urban morphology indicators were selected with reference to the existing literature [38,39], as well as being based on urban planning regulation, specifically including BCR, BH\_mean, FAR, and SVF\_mean within a unit grid (Table 3). These indicators cover the attribute characteristics of buildings in four aspects, density, height, intensity of spatial development, and openness of view, and more comprehensively characterize the built morphology within the city, both horizontally and vertically. Fishnets were created with the help of ArcGIS 10.2.0.3348 software, calculations were performed with a unit grid as the smallest study unit, and urban morphology indicators within each grid were calculated by the field calculator.

**Table 3.** Definition and calculation formula of urban morphological indicators.

Indicator	Definition	Computing Formula	Description
Building coverage ratio (BCR)	The ratio of total building footprint area in a unit grid to unit grid area	$BCR_i = \frac{M_i}{A}$	Where $i$ is the $i$ th unit grid; $M$ is the total area of building footprint in a unit grid; $A$ is the area of a unit grid(%)
Mean building height (BH_mean)	The mean height of buildings in a unit grid	$BH\_mean_i = \frac{H_i}{j}$	Where $H$ is the sum of the height of buildings in the $i$ th unit grid; $j$ is the number of buildings in a unit grid(m)
Floor area ratio (FAR)	The ratio of total floor area to unit grid area	$FAR_i = \frac{\sum_{j=1}^n (E_j \times F_j)}{A}$	Where $j$ is the $j$ th building in a unit grid; $E$ is the floor area of a building in a unit grid; $F$ is the number of floors of a building in a unit grid(%)
Mean sky view factor (SVF_mean)	The ratio between the radiation received by a planar surface and the entire hemispheric radiating environment	$SVF_i = 1 - \sum_{i=1}^N \sin^2 \beta \left( \frac{a_i}{360^\circ} \right)$ $SVF\_mean_i = \frac{SVF_i}{n}$	Where $N$ is the total number of sectors in the sky hemisphere that are obscured by obstacles; $\beta$ is the angle of maximum building height of each sector; $a_i$ is the azimuthal angle of each sector(%)

#### 2.5. Geographically Weighted Regression Model

GWR is a modeling method proposed by Brunson et al. [40] for the spatial non-stationarity of variables, and it is a more commonly used spatial analysis technique. Based on nonparametric local weighted regression, the GWR model establishes a local regression equation at each spatial position in the study area and reflects the changes of dependent variables at each spatial position through regression coefficients. To a large extent, the GWR model solves the spatial heterogeneity problem ignored by traditional regression models

when performing LST downscaling, and it reveals the spatial location differences of local models [41]. The model equation is:

$$Y_i = \beta_0 (u_i, v_i) + \sum_{k=1}^n \beta_k (u_i, v_i) x_{ik} + \varepsilon_i \quad (12)$$

where:  $Y_i$  denotes the mean LST at the  $i$ th position;  $\beta_0 (u_i, v_i)$  is a constant term;  $n$  represents the number of urban spatial pattern indicators;  $x_{ik}$  denotes the value of each urban spatial pattern indicator at the  $i$ th position;  $\beta_k (u_i, v_i)$  is the regression coefficient of each urban spatial pattern indicator at the  $i$ th point; and  $\varepsilon_i$  is the random error term at the  $i$ th position.

Finally, the workflow framework of this study is shown in Figure 2.

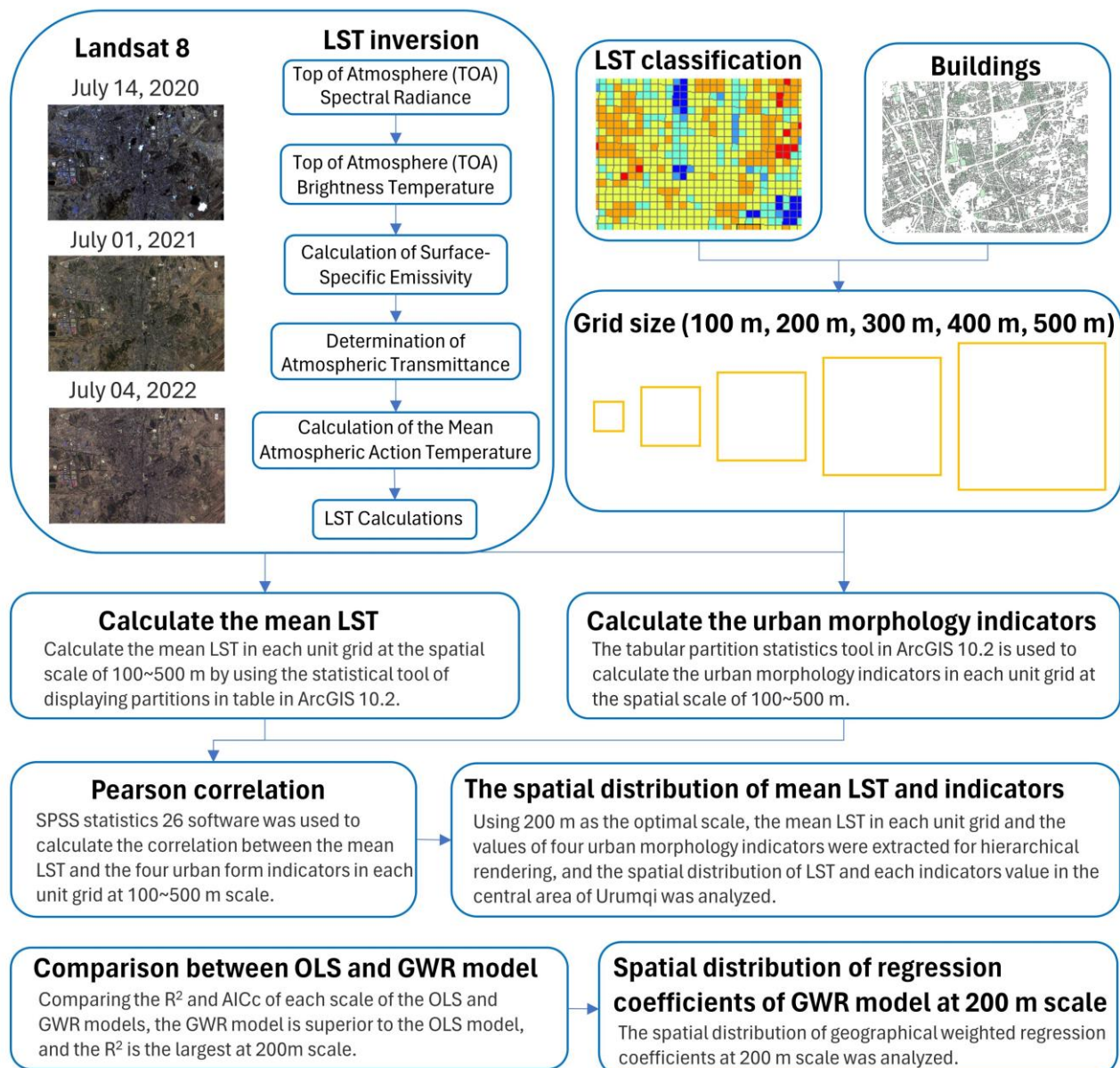


Figure 2. Research framework.

### 3. Results

#### 3.1. Selection of Optimal Spatial Scale

In order to find the best spatial scale for the relationship between urban morphology and LST, we refer to the existing studies and create 100-m, 200-m, 300-m, 400-m, and 500-m fishnets based on the basal area of the urban buildings, calculate the urban morphology



indicators in the grids of each scale, and then extract the mean value of the LST of the three years in the grids. Then, Pearson's correlation analysis of the five spatial scales for the urban morphology indicators and the mean LST are carried out (Figure 3). At the 300-m scale, the correlation between BCR, FAR, and LST is the largest, but the correlation between SVF\_mean is weaker. At the 400-m scale, the correlation between BH\_mean, SVF\_mean, and LST is the largest, but the correlation between BCR and FAR is at the back of five scales, although the correlation between each indicator and LST at 200 m is not the most significant, but the correlation between four indicators and LST are all significant, so this paper chose 200 m as the best spatial scale.

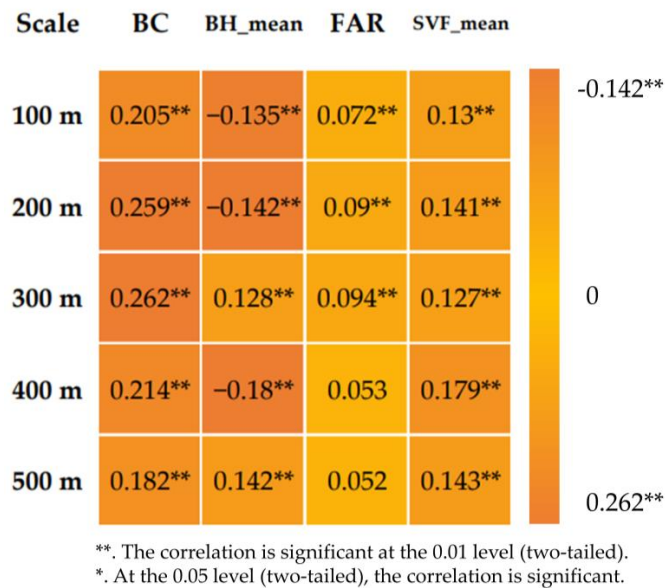


**Figure 3.** Heat map of Pearson's correlation coefficient between urban morphology indicators and LST.

### 3.2. Distribution Characteristics of LST and Urban Morphology Indicators

#### 3.2.1. Characterization of the LST Spatial Distribution

According to the standard deviation method, the summer LST in the central urban area of Urumqi was graded and the spatial distribution pattern of LST was analyzed. In summer, the EHLZ (45.30~48.85 °C) accounts for 2.21% of the total area and is distributed piecemeal (Figure 4). The EHLZ is dominated by low-rise buildings with steel-colored roofs or lighter colors, densely packed buildings, and less green areas. The HLZ (41.18~45.30 °C) accounts for 26.08% of the total area and is distributed in a piecemeal manner, which consists of large areas of impermeable surface as well as densely packed medium- to low-rise buildings, which form fewer shadows under solar irradiation due to limited height, low vegetation cover, and a large amount of anthropogenic heat emissions. The RHLZ (37.06~41.18 °C) accounts for 53.01% of the total area, which is dominated by medium-rise and high-rise buildings, mostly in neighborhoods with high levels of greenery, and high-rise buildings that form shadows under solar irradiation, which reduces the LST to a certain extent. MLZ (32.94~37.06 °C) and RLLZ (28.82~32.94 °C) accounted for 12.42% and 2.88% of the total area, respectively, and were distributed around the LLZ, which is mostly high-rise buildings with a large spacing of buildings and high level of greenery or well-greened scenic areas. The LLZ (6.95~28.82 °C) accounts for 3.4% of the total area and is mainly found in botanical gardens and parks, etc., such as Ertong Park, Renmin Park, and Yamalike mountain in the Shayibake district; Hongshan Park and Shuimogou Park in the Shuimogou district; South Park in the Tianshan district; and Honghu Campus of Xinjiang University, etc. These areas are mainly urban parks, squares, and scenic spots, with a high level of greenery, and urban bodies of water, which indicates that vegetation and water bodies have an obvious cooling

effect. In general, the summer LST in Urumqi ranges from 6.95 °C to 48.85 °C, with a wide temperature range. The summer LST in the central urban area is high, with 81.29% of the area in the RHLZ and above, and a smaller area in the MLZ, RLLZ, and LLZ.

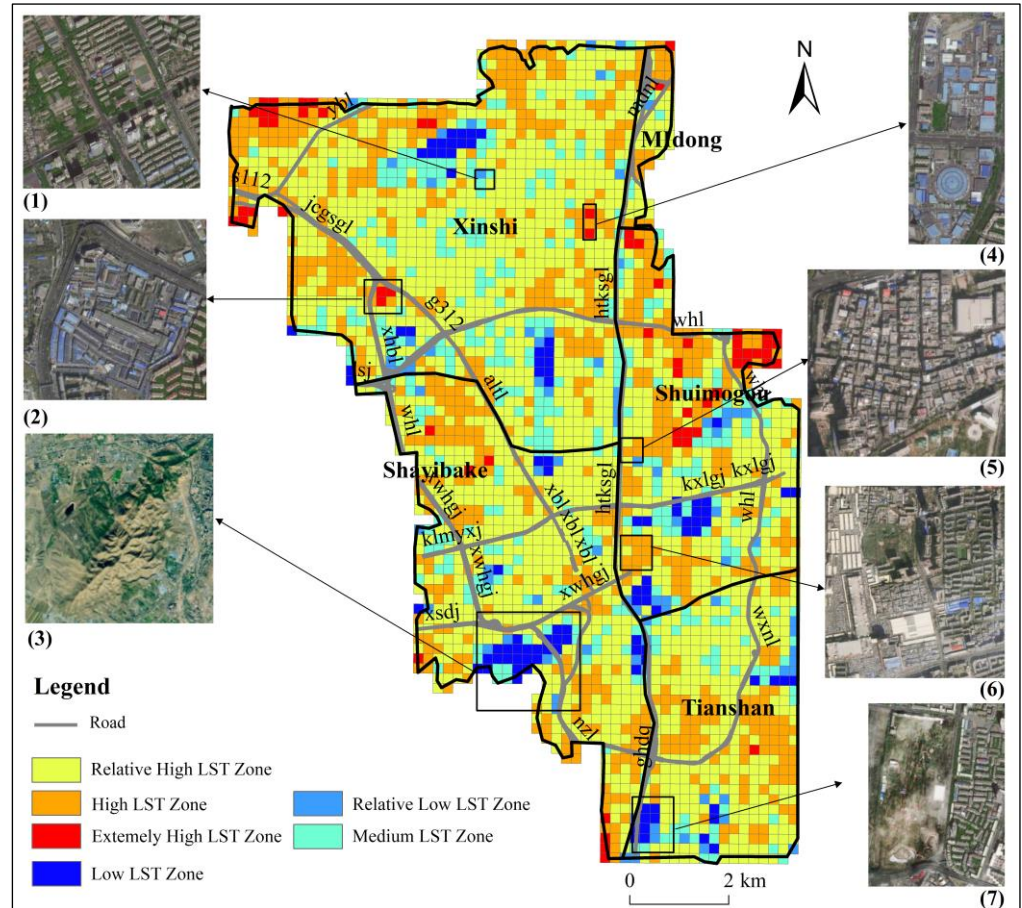


**Figure 4.** Spatial distribution of summer mean LST grades (°C) and corresponding urban morphology imageries, (1)–(7), in the central urban area of Urumqi at 200-m scale.

### 3.2.2. Characteristics of the Spatial Distribution of Urban Morphology Indicators

Figure 5 shows the BCR, BH\_mean, FAR, and SVF\_mean in the central urban area of Urumqi at a spatial scale of 200 m. The BCR, BH\_mean, and FAR show the distribution characteristics of “high in the middle and low in the surroundings” and the SVF\_mean shows the distribution of “low in the middle and high in the surroundings”. The high BCR values (>0.57) are mainly distributed in Hualing Mall on the right side of the Hetan road in the Shuimogou district and on the north and south sides of the outer ring road in the Xinshi district. Meanwhile, the low BCR values (<0.27) are distributed in the outermost layer, which is mostly a large area of open spaces, mountains, and farmland, etc. The BH\_mean high values (>22 m) are centrally distributed around the right side of the Hetan road in Tianshan district and the right side of Baoshan road around the South Railway Station in Shayibake district, with a large number of high-rise office and residential buildings, and there are also some high-value distributions in the Xinshi district, which is dominated by high-rise residential areas; the low BH\_mean values (<14 m) are mainly distributed in the Xinshi, Shayibake, and Midong districts. The FAR high-value (>3.01) area is mainly distributed in the Tianshan district, and also scattered in the Shayibake district, Shuimogou district, and Xinshi district, where the buildings are dense and the mean height is high and the land development intensity is high. The low values (<1.00) are mainly distributed in the Midong district, Xinshi district, and Shayibake district; the low SVF\_mean values (<0.79) are mainly distributed on both sides of the Hetan road at the border between the Shayibake

and Tianshan districts, which is mainly a central commercial and residential area; and the high SVF\_mean values (>0.87) are distributed in the fringe zones in the Xinshi district, Midong district, and Shayibake district. In general, at the 200-m spatial scale, the BCR in the central urban area of Urumqi is relatively dense; BH\_mean is generally low, with mainly low- and medium-rise buildings; the intensity of land development is strong; and the SVF\_mean is high in most areas and smaller in some areas of the central commercial area and old residential areas, with an overall trend of a gradual increase from the center to the surroundings.

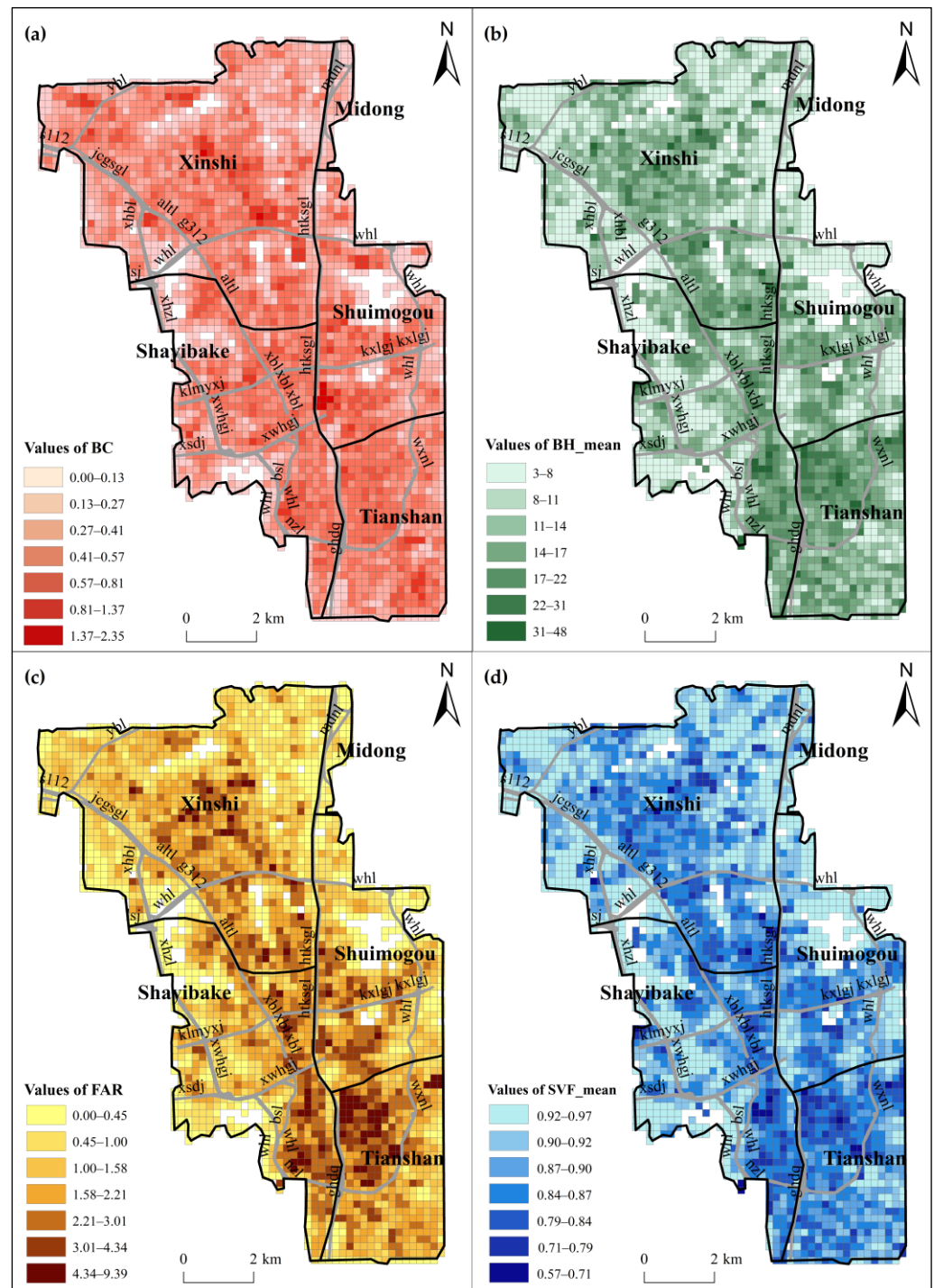


Figure 5. Spatial distribution of four indicator values: (a) BCR; (b) BH\_mean; (c) FAR; (d) SVF\_mean.

### 3.3. Analysis of the Impact of Urban Morphology Indicators on LST

#### 3.3.1. Comparison of the OLS and the GWR Model

Using the 100~500-m resolution grid mean LST as the dependent variable and the urban morphology indicators as the independent variables, the OLS regression model and the GWR model were established, and the fitting degree of the two models was compared. Firstly, the OLS model calculates the influence of four urban morphology indicators on LST, and the variance inflation factor (VIF) is used to determine whether there is multicollinearity among the variables and whether the VIF values of the independent variables are all less than 7.5, which indicates that there is no significant multicollinearity between the independent variables. As can be seen from Table 4, the adjusted  $R^2$  of both the OLS model and the GWR model first increases and then decreases with the increase in the spatial scale, in which the OLS model achieves the maximum value of 0.119 at a spatial scale of 400 m. From a global perspective, the variables' explanatory power of the LST is only 11.9%, and the AICc is larger, which is not a desirable fitting effect. Before establishing the GWR model, the LST was tested for the existence of spatial autocorrelation, and the global Moran's index of the LST was calculated to be 0.432 using ArcGIS 10.2.0.3348 and significant at the 1% level, which indicates that the grid mean LST has strong spatial autocorrelation and meets the conditions for carrying out GWR analyses. The  $R^2$  of the GWR model adjusted on the 200-m spatial scale reached a maximum value of 0.396, indicating that the GWR model has stronger explanatory power than the OLS model, and again indicating that 200 m is the best spatial scale. By comparing the local regression coefficients of each urban morphology indicator in the regression results of the GWR model, the results show that the median and mean of the local regression coefficients take similar values and have the same sign, which indicates that the effects of the four urban morphology indicators on LST are more consistent in most regions; at the same time, the changes in of the regression coefficients reflect the differences and imbalances of the effects of the urban morphology indicators on LST in the space (Table 5).

**Table 4.** Comparison between OLS and GWR model.

Scale	OLS		GWR	
	AdjR <sup>2</sup>	AICc	AdjR <sup>2</sup>	AICc
100 m	0.06	53,203.39	0.380	49,373.13
200 m	0.105	14,669.77	0.396	13,688.73
300 m	0.107	6676.82	0.325	6353.53
400 m	0.119	3763.88	0.284	3629.37
500 m	0.084	2590.84	0.183	2540.70

**Table 5.** GWR results for mean LST and urban morphology indicators at the 200-m scale.

Indicator	Mean	Median	Min	Max	S.D.
BCR	6.524	4.837	−6.109	28.442	5.665
BH_mean	−0.312	−0.104	−0.523	0.313	0.143
FAR	0.032	0.021	−2.529	3.524	1.047
SVF_mean	−1.005	−1.086	−14.660	10.106	4.075

#### 3.3.2. Analysis Based on GWR Models

The visualization of regression coefficients (Figure 6) shows that the effects of BCR, BH\_mean, FAR, and SVF\_mean on surface temperature are spatially unstable, and all four indicators have a certain ability to increase and decrease the temperature and show the spatial distribution characteristics of agglomeration. According to the regression coefficient, it can be seen that the degree of influence of the four indicators on LST is BCR > SVF\_mean > FAR > BH\_mean. Combining the Baidu map, the distribution characteristics of the urban

morphology indicators, and the distribution characteristics of LST, we analyze the influence of the four indicators on LST individually.

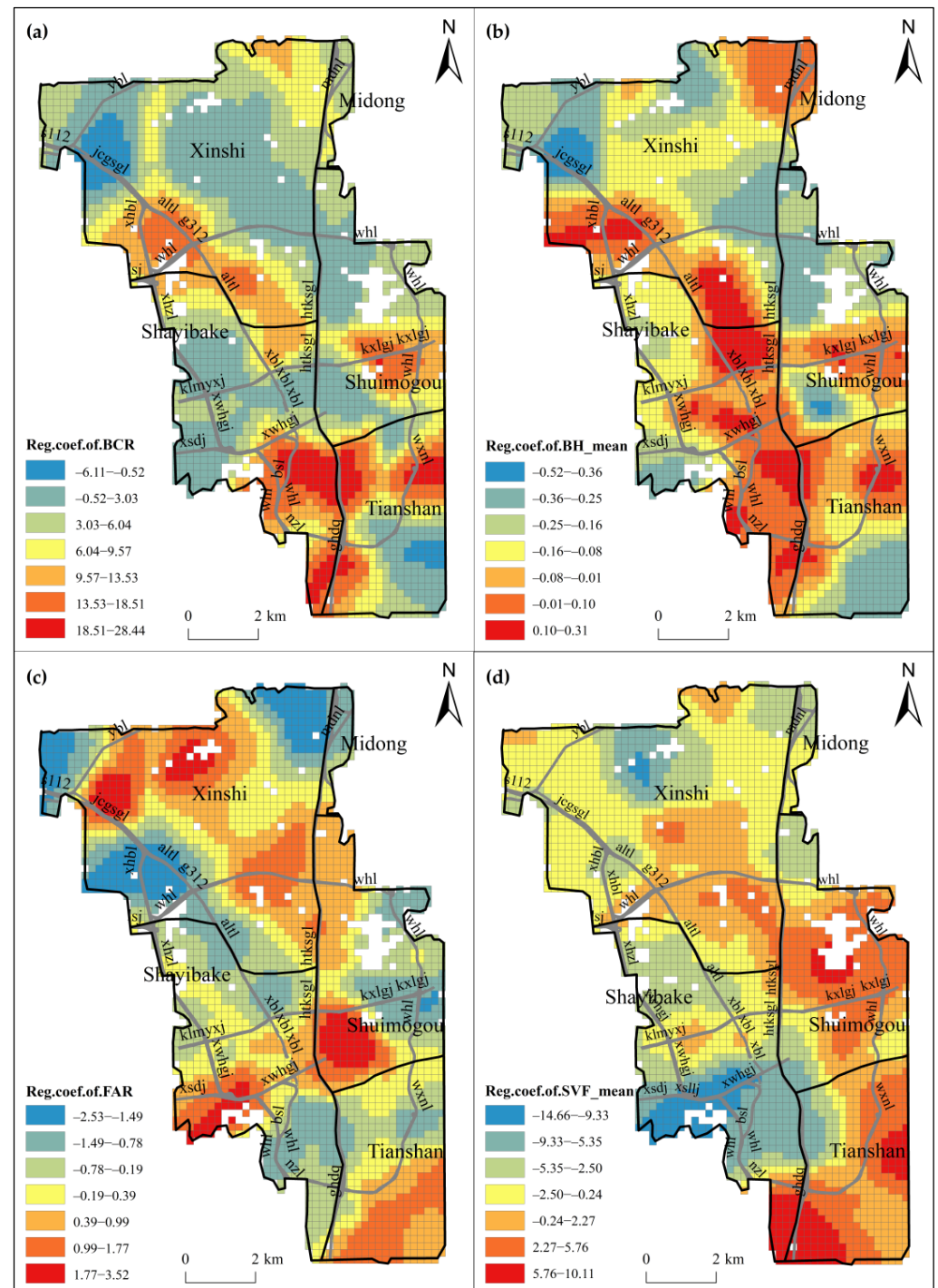


**Figure 6.** Spatial distribution of regression coefficients of GWR model: (a) regression coefficients of BCR; (b) regression coefficients of BH\_mean; (c) regression coefficients of FAR; (d) regression coefficients of SVF\_mean.

The BCR showed a significant warming effect in more than 66% of the area, and the areas with large regression coefficients and strong warming effects were concentrated in the area around the timber factory overpass in the Xinshi district, east of Aletai road, both sides of the Hetan road at the junction of the Shayibake and Tianshan districts, and both

sides of the Kexi road in the Shuimogou district, with a regression coefficient of 18.51, suggesting that a 1% increase in the BCR within a 200-m grid would result in the grid mean LST increasing by more than 0.18 °C (regression coefficient > 18.51). These areas consist of densely packed buildings with little distance between them (narrow streets). Any wind speed in the narrow street will be reduced by the buildings in the surrounding area, so the air circulation efficiency in the area will be reduced and the LST will be increased to some extent. Secondly, this area has low vegetation coverage, low reflectance, high heat capacity, high thermal conductivity, and increased LST. The high traffic flow in this area, the large amount of vehicle exhaust, human-generated heat, and the inability to diffuse over time are also reasons for the increase in the LST. Less than 34% of the area has a negative correlation between BCR and LST, mainly in the north of the outer ring road in the Xinshi district, the border zone between Shayibake and Shuimogou districts, and the southeast of Tianshan district, which are characterized by two types of buildings: in the first type, the buildings are more densely spaced but also have a larger area of greenery, which mitigates a certain amount of LST; in the second type, the buildings are less densely spaced but have less greenery, with a high proportion of impermeable surfaces, which caused an elevated LST.

The BH\_mean has a significant attenuating effect on the LST, which is due to the fact that high-rise buildings form larger shadows under the sun's irradiation, and these shadows cover the ground surface and reduce the LST. Approximately 91% of the areas show the feature that the higher the building is, the lower the LST is; for example, both sides of the airport highway in the Xinshi district, west of the Hetan road, east of the Hetan Road in Shuimoqou district, and the junction between Shayibake district and Tianshan district. Approximately 9% of the areas show the phenomenon of warming, such as in the Shuimoqou district and most of the Xinshi district, which is probably due to the fact that the areas are mainly populated with low-rise buildings that do not form large shadows, and the area receiving solar radiation is larger, resulting in a higher LST.

According to the regression coefficient, the FAR has a bidirectional regulating effect on LST, and the FAR is positively correlated with LST in 54% of the region, such as around the Botanical Garden and Meiju in the Xinshi district, Hualing in the Shuimogou district, and around the South Railway Station in the Shayibake district, which is probably due to the fact that the areas with high building intensities have more buildings, contain more population, and have more human activities and anthropogenic heat releases, and the higher buildings used for cooling or heating produce more energy consumption, thus generating a higher LST. In 46% of the areas, FAR and LST are negatively correlated, probably because, where the building intensity is not high, there are fewer human activities and less anthropogenic heat release, e.g., the northwest of Yingbin road in the Xinshi district and the Shuimogou district. On the other hand, it could also be because the higher the building height in the area with a larger plot ratio, the larger the shadow area that is formed. Consequently, this reduces the LST, such as around the Nanmen in the Xinshi district.

For the SVF\_mean, approximately 60% of the region's SVF\_mean is negatively correlated with LST and approximately 40% of the region's SVF\_mean is positively correlated with LST. The impact of SVF\_mean on LST is mainly manifested in two ways. First, the higher the SVF\_mean is, the lower the surface temperature is. This is because the more open the urban buildings are, which is conducive to air flow, the more LST will be reduced. Second, the higher the SVF\_mean, the higher the surface temperature. A higher SVF\_mean indicates that BCR and impervious surfaces are both higher, and more solar radiation reaches the surface. For example, near the outer ring line of the Shayibake district, the buildings are dense and the impervious ground area is large and can therefore receive a large amount of solar radiation, resulting in a high LST.

## 4. Discussion

### 4.1. Two Approaches to Optimal Spatial Scale Selection

In the study of the relationship between urban morphology indicators and LST, spatial scale selection is an important prerequisite. Currently, scholars determine the spatial scale in

two ways. One method is by establishing multiple resolution fishnets, calculating the mean LST and urban morphology indicator values in individual grids, and by comparing the Pearson correlation coefficients between the mean LST and urban morphology indicators in individual grids, selecting the grid scale where the correlation between the LST and all the indicators is the largest. By comparing other studies, the optimal spatial scales for the study of urban morphology and LST are different for different cities; for example, this study found that 200 m is the optimal scale for the correlation between urban morphology indicators and LST in Urumqi by comparing five types of resolution grids. Guo et al. [38] chose ten spatial grid scales (30~570 m), with intervals of 60 m. By comparing the grid scales of the urban morphology indicators with the mean LST, it was found that 510 m was the best spatial scale for the correlation between urban morphology indicators and LST in Chongqing city. By comparing six spatial scales (90~540 m), Yuan et al. [39] found that 450 m was the best scale to study the urban building morphology and LST in Nanjing city. Han et al. [42] found that 270 m was the best scale to study the urban morphology and LST of Beijing. Firstly, this may be due to the differences in BCR and BH in each city, which have different economic levels, and secondly, the topographic and climatic background of the city may also contribute to the differentiation of the study results. There are also some studies that show that, even in the same city with different spatial scales, the influence of urban morphology indicators on LST is different. For example, when Tianjin city is divided into a 120-m scale grid, water body percentage, green land rate, and BH are negative contribution indicators, while impermeability, SVF, and BCR are positive contribution indicators. FAR has a bidirectional regulating effect on LST, while when Tianjin city is divided into a 600-m scale grid, BCR, FAR, and LST are positively correlated. BH and SVF are negatively correlated with LST [43,44]. This may be due to the fact that, at the 120-m scale, the taller buildings in some grids block solar radiation, which puts some of the buildings in shadow and is not conducive to demonstrating more spatial variations in LST. As the spatial scale increases, the changes caused by spatial variations in the 3D morphology of buildings are relatively smaller and the buildings are able to demonstrate more spatial variations in LST. Compared with first-tier cities such as Chongqing, Beijing, and Tianjing, Urumqi has a sparser BCR and a lower mean BH, so the optimal study scale is smaller than that of the above cities. The second approach is to explore the relationship between urban morphology and LST with the community or planning management unit as the smallest research unit. The planning management unit is the basic unit of urban construction, controlling land use and development intensity, and plays a very important role in supervising the implementation management of policies in the planning process [13,45]. The conclusions obtained by using the planning management unit as a research scale can better guide urban planning and construction, but the disadvantage is that it is difficult to obtain the administrative map of the planning and management unit. There are no reports in the literature as yet to prove which of these two approaches is better, and which should be the direction for future research.

#### *4.2. Differential Impact of Urban Morphology Indicators on LST in Different Cities*

A large number of studies have quantified urban morphology into different indicators to explore its impact on LST, and the results are different due to the different study areas. In this paper, we found that all four indicators have different degrees of warming and cooling effects on LST, such as BCR and FAR having more significant warming effects, while FAR and SVF show obvious cooling effects in most regions. Zeng et al. [46] found that mean architecture height, BCR, high-building ratio, vegetation coverage ratio, and architecture height standard deviation are the main indicators affecting LST, with relative contributions of 24.8%, 14.9%, 14.7%, 8.2%, and 7.6%, respectively. This is similar to the findings of this paper. Sun et al. [47] found that, in summer, BCR, BH\_mean, mean architecture height standard deviation (AHSD), and mean architecture projection area (MAPA) were the most influential factors, which is consistent with some of the findings of this study. The reason for this is because, in general, the higher the BCR and BH, the poorer the urban ventilation

performance of the city; it is not easy to emit heat, and when the BH is higher, the SVF is generally smaller, the FAR value is larger, and the building produces a larger shadow area under the sun's irradiation, which reduces the LST. However, there are some pieces of research that show that the effects of BH, SVF, and FAR, as indicators for LST, are different from those in this paper. For example, Guo et al. [38] showed that the correlation between FAR and LST was not significant in Chongqing, which may be due to the fact that different building plots have the same FAR values, and furthermore, open high-rise buildings have larger shadows in sunlight, which makes the relationship between FAR and LST insignificant. Guo et al. [5] found that medium SVF values produce the lowest LST, while maximum and minimum SVF values produce the highest LST in Guangzhou. The above studies show that the same urban morphology indicators have different impacts on the LST in different cities, which is due to different background conditions, such as climatic conditions, economic levels, and the population size of each city, which leads to different levels of urban development. The second reason arises on the basis of the first one: the building layouts of each city are very complex and different, with varying building areas, heights, and densities, as well as green space areas, impervious surface areas, and other elements that are combined into a different morphology. Even if the indicators are the same, the values within the statistical units are different, leading to the variability in the results.

## 5. Conclusions and Outlook

In this paper, the LST of the central urban area of Urumqi is taken as the study area, the mono-window algorithm is used to invert the LST of the study area, and the standard deviation method is used to classify the LST to explore its spatial distribution pattern. It is found that the LST of Urumqi in summer ranges from 6.95 to 48.85 °C, with a large span of temperature difference, and the LST of the central urban area is on the high side in summer. The mean LST and urban morphology indicators were calculated by creating five kinds of resolution grids, from 100 m to 500 m. By comparing Pearson's correlation coefficients, it was found that 200 m was the optimal spatial scale for the study of LST and urban morphology in Urumqi. Based on the OLS model and GWR model to analyze the relationship between BCR, BH\_mean, FAR, SVF\_mean, and LST, it is found that the LST has spatial heterogeneity, the OLS model is not able to reflect the spatial instability of the urban morphology indicators in relation to the LST, and the GWR model is more suitable for the study of urban morphology's influence on the LST. The regression coefficients of the GWR model show that the four indicators have different warming and cooling abilities in relation to the LST in different spatial regions. Among them, BCR, FAR, and SVF\_mean have a warming effect on the LST in most areas, and BH\_mean has a negative correlation with the LST and has a cooling effect in most areas. According to the above results, we have proposed some possible planning suggestions for mitigating the UHI effect in Urumqi. First, the BCR around Times square in the Tianshan district, Nanhu square in the Shuimogou district, and Mucaichang market in the Xinshi district should be specially reduced to promote the circulation and dissipation of anthropogenic heat. Second, in future urban planning, the shading function of buildings should be effectively used around Hualing Automobile market in the Shuimogou district and near the botanical garden in the Xinshi district, thereby appropriately increasing BH and reducing SVF to obtain greater surface shading and alleviating the UHIs. Finally, in future urban planning, the proportion of ecological cooling sources, such as water bodies and green spaces, should be reasonably allocated in high-density building areas such as Youhao road in the Shayibake district and Renmin square in the Tianshan district, so as to reduce the heat cycle between buildings and the surrounding landscape and reduce the surrounding temperature. In addition, the orientation of buildings should be rationally planned with reference to the wind direction and solar radiation of Urumqi to create a suitable urban ventilation corridor.

In this paper, we studied the effects of BCR, BH\_mean, FAR, and SVF\_mean on LST and have drawn some meaningful conclusions, but there are some limitations: (1) this paper only considers the effect of urban morphology on the summer daytime LST and does



not consider other seasons; (2) we only selected four urban morphological parameters and ignored the impact of quantifying urban ventilation performance on LST; (3) we did not consider the vertical typology based on different combinations or precinct ventilation zone typology on the basis of the LCZs scheme. These are the directions of potential studies and need to be further advanced in future work.

**Supplementary Materials:** The following supporting information can be downloaded at <https://www.mdpi.com/article/10.3390/su152115255/s1>. Table S1: values of LST\_mean, building density, building height, floor area ratio, and sky view factor at 100-m to 500-m spatial scale.

**Author Contributions:** Conceptualization, J.F. and X.C.; methodology, J.F. and S.X.; software, J.F. and S.X.; validation, J.F., X.C. and Y.Z.; formal analysis, J.F.; resources, Y.Z.; data curation, J.F.; writing—original draft preparation, J.F.; writing—review and editing, J.F.; visualization, J.F.; supervision, X.C.; funding acquisition, X.C. and Y.Z. All authors have read and agreed to the published version of the manuscript.

**Funding:** The research was sponsored by the Natural Science Foundation of Xinjiang Uygur Autonomous Region (No.2022D01A212).

**Institutional Review Board Statement:** Not applicable.

**Informed Consent Statement:** Not applicable.

**Data Availability Statement:** The data presented in the study are available in the Supplementary Materials.

**Acknowledgments:** We are grateful to the National Catalogue Service for Geographic Information, the USGS Data Center, and the Geospatial Data Cloud for providing us with the foundational data.

**Conflicts of Interest:** The authors declare no conflict of interest.

## References

1. UN-Habitat. World Cities Report 2016: Urbanization and Development-Emerging Futures. Available online: <https://unhabitat.org/world-cities-report-2016> (accessed on 24 June 2023).
2. Kalnay, E.; Cai, M. Impact of urbanization and land-use change on climate. *Nature* **2003**, *423*, 528–531. [[CrossRef](#)]
3. Li, Y.F.; Schubert, S.; Kropp, P.J.; Rybski, D. On the influence of density and morphology on the Urban Heat Island intensity. *Nat. Commun.* **2020**, *11*, 2647. [[CrossRef](#)]
4. He, B.J.; Ding, L.; Prasad, D. Enhancing urban ventilation performance through the development of precinct ventilation zones: A case study based on the Greater Sydney, Australia. *Sustain. Cities Soc.* **2019**, *47*, 101472. [[CrossRef](#)]
5. Guo, G.H.; Zhou, X.Q.; Wu, Z.F.; Xiao, R.B.; Chen, Y.B. Characterizing the impact of urban morphology heterogeneity on land surface temperature in Guangzhou, China. *Environ. Modell. Softw.* **2016**, *84*, 427–439. [[CrossRef](#)]
6. Rao, P.; Tassinari, P.; Torreggiani, D. Exploring the land-use urban heat island nexus under climate change conditions using machine learning approach: A spatio-temporal analysis of remotely sensed data. *Heliyon* **2023**, *9*, e18423. [[CrossRef](#)]
7. Li, X.X.; Norford, K.L. Evaluation of cool roof and vegetations in mitigating urban heat island in a tropical city, Singapore. *Urban. Clim.* **2016**, *16*, 59–74. [[CrossRef](#)]
8. Tian, L.; Li, Y.C.; Lu, J.; Wang, J. Review on Urban Heat Island in China: Methods, Its Impact on Buildings Energy Demand and Mitigation Strategies. *Sustainability* **2021**, *13*, 762. [[CrossRef](#)]
9. Bai, X.M.; Shi, P.J.; Liu, Y.S. Realizing China's Urban dream. *Nature* **2014**, *509*, 158–160. [[CrossRef](#)]
10. Zheng, Y.H.; Huang, L.; Zhai, J. Divergent trends of urban thermal environmental characteristics in China. *Clean. Prod.* **2021**, *287*, 125053. [[CrossRef](#)]
11. Cai, Z.; Demuzere, M.; Tang, Y.; Wan, Y.M. The characteristic and transformation of 3D urban morphology in three Chinese mega-cities. *Cities* **2022**, *131*, 103988. [[CrossRef](#)]
12. Zhang, P.; Ghosh, D.; Park, S. Spatial measures and methods in sustainable urban morphology: A systematic review. *Landscape Urban. Plan.* **2023**, *237*, 104776. [[CrossRef](#)]
13. Lu, Y.P.; Yue, W.Z.; Huang, Y.P. Effects of Land Use on Land Surface Temperature: A Case Study of Wuhan, China. *Int. J. Environ. Res. Public Health* **2021**, *18*, 9987. [[CrossRef](#)]
14. Bokaie, M.; Zarkesh, M.K.; Arasteh, P.D.; Hosseini, A. Assessment of Urban Heat Island Based on the Relationship between Land Surface Temperature and Land Use/Land Cover in Tehran. *Sustain. Cities Soc.* **2016**, *23*, 94–104. [[CrossRef](#)]
15. Hamoodi, M.N. Investigating the Effects of Armed and Political Conflicts on the Land Use/Cover Change and Surface Urban Heat Islands: A Case Study of Baghdad, Iraq. *J. Indian Soc. Remote* **2021**, *49*, 1493–1506. [[CrossRef](#)]

16. Myint, S.W.; Zheng, B.J.; Talen, E.; Fan, C.; Kaplan, S.; Middel, A.; Smith, M.; Huang, H.P.; Brazel, A. Does the spatial arrangement of urban landscape matter? Examples of urban warming and cooling in Phoenix and Las Vegas. *Ecosyst. Health Sust.* **2015**, *58*, 261–280. [[CrossRef](#)]
17. Kim, J.I.; Jun, M.J.; Yeo, C.H.; Kwon, K.H.; Hyun, J.Y. The Effects of Land Use Zoning and Densification on Changes in Land Surface Temperature in Seoul. *Sustainability* **2019**, *11*, 7056. [[CrossRef](#)]
18. Banerjee, S.; Ching, C.N.Y.; Yik, S.K.; Dzyuban, Y.; Crank, J.P.; Rachel, P.X.Y.; Chow, T.L.W. Analyzing impacts of urban morphological variables and density on outdoor microclimate for tropical cities: A review and a framework proposal for future research directions. *Buuld. Environ.* **2022**, *225*, 109646. [[CrossRef](#)]
19. Chen, Y.; Yang, J.; Yu, W.B.; Ren, J.Y.; Xiao, X.M.; Xia, C.J.H. Relationship between urban spatial form and seasonal land surface temperature under different grid scales. *Sustain. Cities Soc.* **2023**, *89*, 104374. [[CrossRef](#)]
20. Liu, Y.; Wang, Z.P.; Liu, X.; Zhang, B.L. Complexity of the relationship between 2D/3D urban morphology and the land surface temperature: A multiscale perspective. *Environ. Sci. Pollut. R.* **2021**, *28*, 66804–66818. [[CrossRef](#)]
21. Zhang, Z.C.; Luan, W.X.; Yang, J.; Guo, A.D.; Su, M.; Tian, C. The influences of 2D/3D urban morphology on land surface temperature at the block scale in Chinese megacities. *Urban. Clim.* **2023**, *49*, 101553. [[CrossRef](#)]
22. Qiao, Z.; Xu, X.L.; Wu, F.; Luo, W.; Liu, L.; Sun, Z.Y. Urban ventilation network model: A case study of the core zone of capital function in Beijing metropolitan area. *J. Clean. Prod.* **2017**, *168*, 526–535. [[CrossRef](#)]
23. He, B.J.; Ding, L.; Prasad, D. Relationships among local-scale urban morphology, urban ventilation, urban heat island and outdoor thermal comfort under sea breeze influence. *Sustain. Cities Soc.* **2020**, *60*, 102289. [[CrossRef](#)]
24. Jiménez-Muñoz, J.C.; Sobrino, J.A. A generalized single-channel method for retrieving land surface temperature from remote sensing data. *Atmospheres* **2003**, *109*, 4688.
25. Chatterjee, R.S.; Singh, N.; Thapa, S.; Sharma, D.; Kumar, D. Retrieval of land surface temperature (LST) from landsat TM6 and TIRS data by single channel radiative transfer algorithm using satellite and ground-based inputs. *Int. J. Appl. Earth Obs.* **2017**, *58*, 264–277. [[CrossRef](#)]
26. Qin, Z.; Dall’Olmo, G.; Karnieli, A.; Berliner, P. Derivation of split window algorithm and its sensitivity analysis for retrieving land surface temperature from NOAA-advanced very high resolution radiometer data. *Atmospheres* **2001**, *106*, 22655–22670. [[CrossRef](#)]
27. Jimenez-Munoz, J.C.; Sobrino, J.A.; Skokovic, D.; Mattar, C.; Cristobal, J. Land Surface Temperature Retrieval Methods From Landsat-8 Thermal Infrared Sensor Data. *IEEE Geosci. Remote. Sens. Lett.* **2014**, *11*, 1840–1843. [[CrossRef](#)]
28. Sobrino, J.A.; Jimenez-Munoz, J.C.; Paolini, L. Land surface temperature retrieval from LANDSAT TM 5. *Remote Sens. Environ.* **2004**, *90*, 434–440. [[CrossRef](#)]
29. Jin, D.D.; Gong, Z.N. Algorithms Comparison of Land Surface Temperature Retrieval from Landsat Series Data: A Case Study in Qiqihar, China. *Remote Sens. Remote Sens. Technol. Appl.* **2018**, *33*, 830–841.
30. Li, B.; Wang, H.; Qin, M.; Zhang, P. Comparative study on the correlations between NDVI, NDMI and LST. *Prog. Geogr.* **2017**, *36*, 585–596.
31. Hu, D.Y.; Qiao, K.; Wang, X.L.; Zhao, L.M.; Ji, G.H. Land surface temperature retrieval from Landsat 8 thermal infrared data using mono-window algorithm. *Natl. Remote Sens. Bull.* **2015**, *19*, 964–976.
32. Su, H.Y.; Han, G.F.; Li, L.; Qin, H.Q. The impact of macro-scale urban form on land surface temperature: An empirical study based on climate zone, urban size and industrial structure in China. *Sustain. Cities Soc.* **2021**, *74*, 103217. [[CrossRef](#)]
33. Yin, C.H.; Yuan, M.; Lu, Y.P.; Huang, Y.P.; Liu, Y.F. Effects of urban form on the urban heat island effect based on spatial regression model. *Sci. Total Environ.* **2018**, *634*, 696–704. [[CrossRef](#)]
34. Zhang, Y.J.; Middel, A.; Turner, L.B. Evaluating the effect of 3D urban form on neighborhood land surface temperature using Google Street View and geographically weighted regression. *Landscape Ecol.* **2019**, *34*, 681–697. [[CrossRef](#)]
35. Qin, Z.H.; Zhang, M.H.; Arnon, K.; Pedro, B. Mono-window Algorithm for Retrieving Land Surface Temperature from Landsat TM6 data. *Acta Geogr. Sin.* **2001**, *56*, 456–466.
36. Qin, Z.H.; Li, W.J.; Xu, B.; Zhang, W.C. The Estimation of Land Surface Emissivity for Landsat TM6. *Remote Sens. Nat. Resour.* **2004**, *22*, 28–36.
37. Yu, D.; Zhou, W.J.; Tan, J.; Guo, Z.C.; Li, J. Temporal and Spatial Variation Characteristics of Land Surface Temperature in Dongting Lake Region, Hunan Province. *Ecol. Environ. Sci.* **2014**, *23*, 1799–1805.
38. Guo, J.M.; Han, G.F.; Xie, Y.S.; Cai, Z.; Zhao, Y.F. Exploring the relationships between urban spatial form factors and land surface temperature in mountainous area: A case study in Chongqing city, China. *Sustain. Cities Soc.* **2020**, *61*, 102286. [[CrossRef](#)]
39. Yuan, S.; Zhang, J.M.; Xu, Z.G.; Tang, G.S.; Wang, C.; Chen, J.K. Response of Urban Heat Island Effect to Morphology Characteristics of Buildings and Its Diurnal Variation. *Geogr. Geo-Inf. Sci.* **2022**, *38*, 40–46.
40. Brunson, C.; Fotheringham, S.A.; Charlton, E.M. Geographically Weighted Regression: A Method for Exploring Spatial Nonstationary. *Geogr. Anal.* **1996**, *28*, 281–298. [[CrossRef](#)]
41. Lu, B.B.; Brunson, C.; Charlton, M.; Harris, P. Geographically weighted regression with parameter-specific distance metrics. *Int. J. Geogr. Inf. Sci.* **2017**, *31*, 982–998. [[CrossRef](#)]
42. Han, D.R.; An, H.M.; Wang, F.; Xu, X.L.; Qiao, Z.; Wang, M.; Sui, X.Y.; Liang, S.Z.; Hou, X.H.; Cai, H.Y.; et al. Understanding seasonal contributions of urban morphology to thermal environment based on boosted regression tree approach. *Buuld. Environ.* **2022**, *226*, 109770. [[CrossRef](#)]

43. Song, X.B.; Huang, H.; Guo, J.; Xiong, M.M. Research on the impact of urban morphology on thermal environment in summer: A case of Tianjin central city. *Ecol. Environ. Sci.* **2021**, *30*, 2165–2174.
44. Song, X.B.; Li, G.; Liang, D.P.; Huang, H.; Guo, J. Relationship between urban spatial morphology factors and land surface temperature in summer: A case of the central district of Tianjing. *Sci. Geogr. Sin.* **2023**, *43*, 360–369.
45. Guo, A.D.; Yang, J.; Xiao, X.M.; Xia, J.H.; Jin, C.; Li, X.M. Influences of urban spatial form on urban heat island effects at the community level in China. *Sustain. Cities Soc.* **2020**, *53*, 101972. [[CrossRef](#)]
46. Zeng, P.; Sun, F.Y.; Liu, Y.Y.; Tian, T.; Wu, J.; Dong, Q.Q.; Peng, S.J.; Che, Y. The influence of the landscape pattern on the urban land surface temperature varies with the ratio of land components: Insights from 2D/3D building/vegetation metrics. *Sustain. Cities Soc.* **2022**, *78*, 13599. [[CrossRef](#)]
47. Sun, F.Y.; Liu, M.; Wang, Y.C.; Wang, H.; Che, Y. The effects of 3D architectural patterns on the urban surface temperature at a neighborhood scale: Relative contributions and marginal effects. *J. Clean. Prod.* **2020**, *258*, 120706. [[CrossRef](#)]

**Disclaimer/Publisher’s Note:** The statements, opinions and data contained in all publications are solely those of the individual author(s) and contributor(s) and not of MDPI and/or the editor(s). MDPI and/or the editor(s) disclaim responsibility for any injury to people or property resulting from any ideas, methods, instructions or products referred to in the content.